Research Square

Preprints are preliminary reports that have not undergone peer review.
They should not be considered conclusive, used to inform clinical practice,
or referenced by the media as validated information.

On the dynamics of lock-exchange flow: coupling viscous evolution and inertial fronts

Mohammadreza Yavari
K. N. Toosi University of Technology
Ali Shahverdi
K. N. Toosi University of Technology
Majid Bazargan
bazargan@kntu.ac.ir

K. N. Toosi University of Technology

Research Article

Keywords: Exchange Flow, Interfacial Flow, Gravity Current, Front Velocity, Miscible Fluids, Displacement Flow, Analytical Solution

Posted Date: May 21st, 2026

DOI: https://doi.org/10.21203/rs.3.rs-9600832/v1

License: This work is licensed under a Creative Commons Attribution 4.0 International License.
Read Full License

Additional Declarations: No competing interests reported.

On the dynamics of lock-exchange flow: coupling viscous evolution and inertial fronts

Mohammadreza Yavari, Ali Shahverdi and Majid Bazargan (bazargan@kntu.ac.ir)

Environmental Engineering Lab, Mechanical Engineering Department,
K. N. Toosi University of Technology, 7 Pardis St., Tehran 1991943344, Iran

Abstract

This study presents an exact solution for horizontal lock-exchange flow in two-dimensional channels, derived directly from the Navier–Stokes equations under the parallel-flow assumption. The formulation provides a closed description of the viscous evolution of the interface between light and heavy fluids and enables its temporal development to be tracked without any empirical closure or approximation. By coupling the viscous solution to a pressure-driven inertial model at the leading edge, a simple and physically consistent method is developed to predict the front velocity. The analysis demonstrates that the front advances according to an inviscid momentum balance, while its thickness and velocity are regulated by viscous redistribution in the main flow behind the front. A key outcome is the identification of two distinct thickness scales—the inertial front thickness and the interface thickness immediately behind the front—which are shown to be independent of density contrast under weakly mixed conditions, despite the density dependence of front velocity. Comparisons with controlled laboratory experiments across a range of Atwood numbers show a very good quantitative agreement. The results also reveal a strong geometric control, with channel height imposing a quadratic time scaling on interface evolution. The compact and physically transparent description of lock-exchange dynamics provided by the analytical framework of this study for horizontal channels can be extended to inclined configurations and related displacement flows.

Keywords: Exchange Flow; Interfacial Flow; Gravity Current; Front Velocity; Miscible Fluids; Displacement Flow; Analytical Solution

Introduction

Gravity currents are referred to flows in which a wedge of relatively dense fluid intrudes into a lighter ambient. They are canonical examples of buoyancy-driven stratified flows and appear in many geophysical and engineering settings such as saline intrusion at canal locks, sediment-laden turbidity currents, atmospheric cold fronts, and volcanic pyroclastic flows. The lock-exchange flow is the case of prime interest in the current study.

Analytical and experimental studies over past decades have shown that lock-exchange and related gravity current problems admit distinct dynamical regimes controlled by the relative importance of buoyancy, inertia, and viscous stresses. Benjamin's classical idealized formulation provided an early inviscid picture of steady gravity current propagation and the associated front condition. [1] Building on that, experimental work of researchers such as Huppert and Simpson [2] established the familiar phase structure of gravity currents — an early "slumping" (inertial) phase followed by viscous-dominated spreading — and quantified how the front propagation depends on the release geometry and fluid properties .

Lock-exchange laboratory experiments and modern diagnostics (PIV, LIF, PLIF) have made it clear that mixing and dissipation at the head and shear layer strongly influence propagation in many practical cases. Shin et al. [3] comprehensive lock-exchange study quantified how dissipation modifies the energy conserving inviscid limit and clarified the role of turbulence in realistic flows. Subsequent inclined tube experiments by Séon et al. [4, 5] documented how the tube tilt, viscous effects and mixing collaborate to produce a sequence of behaviors shifting from near-vertical to near-horizontal orientations — from strong buoyant penetration to parallel counter-currents and viscous dominance — and highlighted regimes in which the front speed is set by local density contrasts rather than simple inviscid balances.

On the theoretical side, much of the classical analytic progress has used shallow-water (two-layer) approximations and energy or momentum balances to obtain front speeds and scaling laws. These approaches capture the large scale inviscid limits and provide valuable intuition. However they require closure hypotheses at the front or layer depths and do not directly deliver full viscous velocity fields or the time-dependent evolution of the internal interface. Recent efforts have therefore pursued complementary directions: (i) viscous/long-wave asymptotic for near-horizontal, buoyancy dominated displacement flows that emphasize the role of viscous fluxes and residual layers; and (ii) exact or semi-exact two-dimensional solutions of the Navier–Stokes

equations under parallel flow assumptions that produce closed-form expressions for velocity, pressure and flux functions in a stratified two-layer geometry [6-9]. As an example of comprehensive viscous regime mathematical study, Taghavi et al. [10] developed viscous-limit analyses for near-horizontal duct displacement flows that elucidate the flux–interface dynamics in the lubrication regime.

A different but powerful analytical avenue — deriving exact two-dimensional solutions of the Navier–Stokes equations under the assumption of locally parallel Poiseuille-like profiles and exploiting those solutions to obtain closed-form flux–interface relations — has recently been advanced and applied to displacement and exchange flows in straight and curved channels. Yavari et al. [11-14] used such exact two-dimensional solutions to derive transient front dynamics and interface evolution in plane channels (including curved ducts) for viscous dominated conditions. These solutions produce the full velocity and pressure fields (within the parallel-flow approximation) and can be directly compared with experiments for small Atwood numbers and weak mixing.

At the other extreme, exact shallow-water solutions and renewed analytical treatments of inviscid two-layer models have recently produced closed form front predictions and clarified the role of front closure conditions. Some studies like Politis and Priede [9] have shown that appropriately posed two-layer shallow-water models can yield exact Riemann-problem solutions that match many features of experiments and high-Reynolds-number regimes.

Beyond classical and shallow-water approaches, several theoretical studies have sought to refine analytical descriptions of gravity and exchange flows by directly addressing viscous, diffusive, and inertial coupling mechanisms. Ungarish and Zemach [15] examined high-Reynolds-number gravity currents and derived closed form asymptotic expressions linking front propagation to the Reynolds and Froude numbers. Cantero et al. [16] developed a simplified theoretical framework coupling buoyancy driven pressure gradients to shear layer entrainment, capturing the transition from laminar to turbulent regimes. Meiburg and Kneller [17] reviewed advances in theoretical and numerical modeling of gravity and turbidity currents, emphasizing the interplay between inertia, density stratification, and viscous diffusion in lock-exchange flows. More recently, van Reeuwijk et al. [18] and Allen et al. [19] analyzed mixing suppression and density- and viscosity-stratified effects in inclined exchange flows, providing theoretical insight into the limits of the Boussinesq

approximation and the role of turbulence closure in momentum balance. Collectively, these works highlight the ongoing efforts to reconcile analytical tractability with the full physics of buoyancy driven exchange flows—a challenge that the present study addresses through an exact Navier–Stokes based formulation.

Taken together, this body of work shows two complementary truths: (i) in viscous-dominated, near-parallel flows the governing equations admit mathematically tractable, highly informative solutions that reveal the interface evolution and viscous fluxes in detail; (ii) once inertia and/or mixing become significant, front dynamics are controlled primarily by local momentum/pressure balances and by how mixing alters the effective density contrast at the leading edge. The present paper embraces these two perspectives. It develops and presents a compact, exact analytical framework (based on a two-dimensional, parallel-flow solution of the Navier–Stokes equations) to compute the time-dependent evolution of the internal interface in horizontal lock-exchange configurations and — by coupling the evolving interface (and its viscous flux) to a simple, physically motivated front momentum balance — to predict the front velocity in the horizontal case. It validates the analytical predictions against new experiments at low Atwood numbers and discusses the range of applicability of the method and how it connects to the inertia dominated limits documented in the experimental literature.

Although only the simple case of two-dimensional horizontal gravity current is analyzed here, the theory is readily available to be applied to arbitrarily chosen configurations and geometries, including inclined exchange or displacement flow. In this study an analytical method for a reliable estimation of the front velocity in a gravity current is presented with the simplest methods and without employing advanced mathematics by employing the physics of the flow.

To enter the analysis, Yavari et al. [12] derived the equations describing the evolution of the interface of viscous flow in 2-D straight and curved channels. Those equations were normalized by the flow rate of the imposed flow as in Taghavi et al. [20], because those studies had considered displacement flow which includes an imposed flow to displace the other fluid. The schematic of the flow considered in Yavari et al. [12] is demonstrated in Fig. 1.

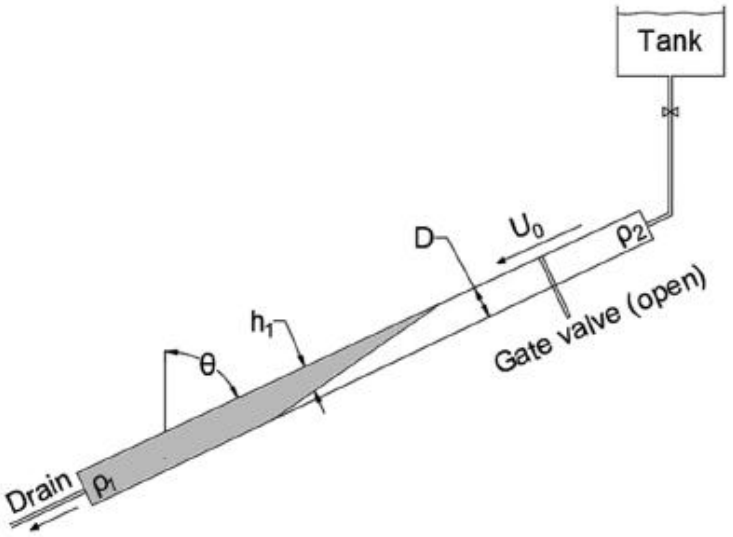


Fig. 1. Schematic of the flow in reference [12]

As demonstrated by Yavari et al. [12], the Navier–Stokes equations can be directly employed to describe both exchange and displacement flows. By enforcing continuity of flow rate, as well as the continuity of velocity and shear stress across the interface, the complete set of governing equations can be formulated. For the specific case of near-horizontal channels where mixing between the two fluid layers is negligible, the governing momentum equation for the denser (heavy) fluid can be derived as Eq. (1). The derivation path toward Eq. (1) is quite lengthy and complicated and is thoroughly addressed in reference [12].

$$Q_2 = \frac{1}{2\mu}\left[-(\rho_1-\rho_2)gsin\theta\frac{\partial h_1}{\partial x}\left(1-\frac{h_1}{D}\right)\left(1+\frac{h_1}{D}-2\frac{h_1^2}{D^2}\right)+(\rho_1-\rho_2)gsin\theta\frac{\partial h_1}{\partial x}\right]\left(-\frac{(D-h_1)^3}{6}\right) + \frac{-(\rho_1-\rho_2)gsin\theta\frac{\partial h_1}{\partial x}\left(1-\frac{h_1}{D}\right)\left(1+\frac{h_1}{D}-2\frac{h_1^2}{D^2}\right)h_1(D-h_1)^2}{-4\mu} + \frac{(\rho_1-\rho_2)gsin\theta\frac{\partial h_1}{\partial x}(D-h_1)^3h_1}{-4\mu D} \qquad (1)$$

Equation (1) can be simplified to obtain Eq. (2) by changing the densities in order to get $Q_2 > 0$, as $\frac{\partial h_1}{\partial x} < 0$ by convention. Also setting $\theta = 90$ indicates the horizontal configuration.

$$Q_2 = \frac{(\rho_2 - \rho_1) g \frac{\partial h_1}{\partial x} (D - h_1)^3}{12\mu} \left[\left(1 - \frac{h_1}{D}\right)\left(1 + \frac{h_1}{D} - \frac{2h_1^2}{D^2}\right) - 1 + \frac{3h_1}{D}\left(1 + \frac{h_1}{D} - \frac{2h_1^2}{D^2}\right) - \frac{3h_1}{D} \right] \qquad (2)$$

As is detailed in reference [12], Eq. (2) can be differentiated with respect to the axial coordinate, to find the equation for evolution of the interface. It leads to Eq. (3) by neglecting the curvature of the interface.

$$\frac{\partial Q_2}{\partial x} = \frac{-(\rho_2 - \rho_1) g \frac{\partial h_1}{\partial x} 3(D - h_1)^2 \frac{\partial h_1}{\partial x}}{12\mu} \left[\left(1 - \frac{h_1}{D}\right)\left(1 + \frac{h_1}{D} - \frac{2h_1^2}{D^2}\right) - 1 + \frac{3h_1}{D}\left(1 + \frac{h_1}{D} - \frac{2h_1^2}{D^2}\right) - \frac{3h_1}{D} \right] + \frac{(\rho_2 - \rho_1) g \frac{\partial h_1}{\partial x} (D - h_1)^3}{12\mu} \left[-\frac{\partial h_1}{D \partial x}\left(1 + \frac{h_1}{D} - \frac{2h_1^2}{D^2}\right) + \left(1 - \frac{h_1}{D}\right)\left(\frac{\partial h_1}{D \partial x} - \frac{4}{D^2} h_1 \frac{\partial h_1}{\partial x}\right) + \frac{3}{D}\frac{\partial h_1}{\partial x}\left(1 + \frac{h_1}{D} - \frac{2h_1^2}{D^2}\right) + \frac{3h_1}{D}\left(\frac{\partial h_1}{D \partial x} - \frac{4}{D^2} h_1 \frac{\partial h_1}{\partial x}\right) - \frac{3\partial h_1}{D \partial x} \right] \qquad (3)$$

Equation (3) can be simplified to get Eq. (4) by some simple algebraic manipulations:

$$\frac{\partial Q_2}{\partial x} = \frac{(\rho_2 - \rho_1) g (\frac{\partial h_1}{\partial x})^2 (D - h_1)^2}{12\mu} \left[\left(1 + \frac{h_1}{D} - \frac{2h_1^2}{D^2}\right)\left(-1 - \frac{8h_1}{D}\right) + \left(1 - \frac{h_1}{D}\right)\left(-2 - \frac{2h_1}{D} - \frac{8h_1^2}{D^2}\right) + 3 + \frac{9h_1}{D} \right] \qquad (4)$$

Equation (4) may be used for the evolution of the interface in horizontal two-dimensional channels. To apply Eq. (4), it is necessary to consider the following relationship to get the time dependent evolution of the interface. It is a simple two-dimensional geometry evolution.

$$\frac{\partial Q_2}{\partial x} = -\frac{\partial h_1}{\partial t} \qquad (5)$$

These equations are consistent with the physics and geometry of the problem considered in this study.

Several key observations can be drawn from the preceding equations. These formulations allow the determination of the flow rate, velocity distribution, and interface evolution at any location along the channel. However, near the advancing front, where inertial effects become dominant, the assumptions underlying these equations no longer hold. A central aspect of this approach is that the temporal variation of the viscous flow behind the front is used to infer the inertial motion that governs the front's advancement.

The novelty of this approach lies in its ability to predict the evolution of the interface at arbitrary positions along the channel. Although the curvature of the interface has been neglected in deriving the governing equations, the formulation remains valid for interfaces with varying local slopes. Specifically, the curvature was neglected only relative to the local slope, thereby permitting nonlinear interface deformation within the analytical framework. In the present study, this formulation is extended to develop a simple yet robust method that couples viscous and inertial flow regimes to estimate the front velocity. The equations derived above describe the viscous region of the flow. However, once the heavier fluid layer encounters the lighter fluid at the leading edge, the dynamics are governed primarily by inertia rather than viscosity. To illustrate this transition, Fig. 2 schematically depicts the motion of a light fluid front advancing into a denser fluid—a phenomenon extensively analyzed in the classical works of von Kármán [21] and Benjamin [1].

As the lighter fluid advances, it displaces the stationary heavier fluid ahead of it, generating a resistance analogous to that experienced by a solid body moving through a fluid. This interaction gives rise to a stagnation region at the leading edge, where the flow decelerates and pressure builds up. The stagnation pressure at this interface—representing the balance between inertial and hydrostatic forces—can therefore be expressed as:

$$P_{Stagnation} = P_{Static} + \frac{1}{2}\rho_H V^2 \qquad (6)$$

Following the basic formulation introduced by Benjamin [1] and later refined by Shin et al. [3], the front velocity is obtained by analyzing a control volume encompassing the frontal region of the flow. A schematic of this control volume, consistent with the approach of Shin et al. [3], is presented in Fig. 2. The pressure distribution along lines CD and BE is assumed to be hydrostatic. While Shin et al. [3] employed a Lagrangian framework in which the control volume moves with

the front, the present analysis adopts an Eulerian perspective, where the control volume remains stationary. The governing equations are evaluated at the instant when the tip of the front is approximately centered within this volume. Although this shift in reference frame does not affect the resulting momentum balance or front velocity, it provides conceptual and computational advantages and ensures consistency with the broader analytical framework.

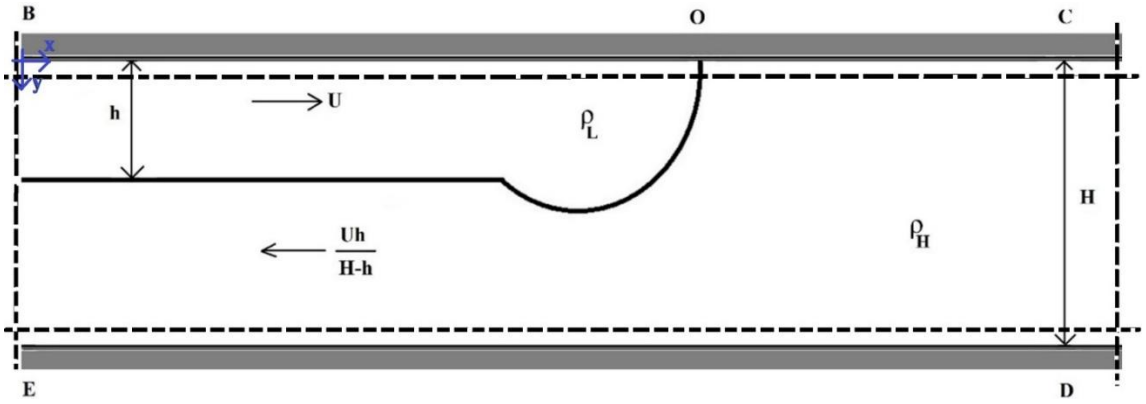


Figure 2 Geometry and control volume used in the current study surrounding the front. The upper layers show the light fluid with velocity U advancing through the heavy fluid.

Considering the pressure along BE and CD, the following momentum equation is formed per Reynolds' transport theorem:

$$\int_0^h \left(P_C + \frac{1}{2}\rho_H U^2 + \rho_L g y\right) dy + \int_h^H (P_C + \frac{1}{2}\rho_H U^2 + \rho_L g h + \rho_H g(y-h)) dy - \int_0^H (P_C + \rho_H g y) dy = -\rho_H U^2 \frac{h^2}{H-h} - \rho_L U^2 h + \frac{\partial}{\partial t}\int \rho u dv \qquad (7)$$

The last term which is the rate of momentum change inside the control volume is given by Eq. (8). Equation (8) represents the momentum change inside the control volume as the fluids have different densities.

$$\frac{\partial}{\partial t}\int \rho u dv = \rho_L U^2 h - \rho_H U^2 h \qquad (8)$$

Performing the integrations denoted in Eq. (7) and using Eq. (8) yields the following equation.

$$\rho_L g\frac{h^2}{2}+\frac{1}{2}\rho_H U^2 H+\rho_L ghH-\rho_L gh^2-\rho_H g\frac{h^2}{2}-\rho_H ghH+\rho_H gh^2$$
$$=-\rho_H U^2\frac{h^2}{H-h}-\rho_H U^2 h \qquad (9)$$

It is possible to solve Eq. (9) for U.

$$\frac{U^2}{gH}=\frac{\left(1-\frac{\rho_L}{\rho_H}\right)(h-2H)(H-h)h}{-H^2(H+h)} \qquad (10)$$

Using the definition $\gamma=\frac{\rho_L}{\rho_H}$, similar calculations may be carried out to obtain the front velocity of the heavy fluid as:

$$\frac{{U_h}^2}{gH}=\frac{\left(\frac{1-\gamma}{\gamma}\right)(h-2H)(H-h)h}{-H^2(H+h)} \qquad (11)$$

It is evident by comparing Eq. (10) and Eq. (11) that the front of the heavy fluid travels faster than the front of the lighter fluid by a factor of $\frac{1}{\gamma}$. For Boussinesq flows ($\gamma \approx 1$), the velocity difference is negligible and the fronts are assumed to move at the same velocity, especially when the interface is located at the middle of the channel. For this reason, U is used interchangeably for the velocity of both fluids. Experimental observations (e.g. Shin et al. [3], Birman et al. [22], Alba et al. [23]) also reveal that the light and heavy front velocities are equal within the experimental uncertainty. In Eq. (11) it is possible to replace *h*, the thickness of the heavy fluid, by h_1 which is the interface distance from the upper wall to be consistent with the notations used in this study. Then the following relationship will be formed for inertial velocity of heavy front.

$$\mathrm{U_i}=\sqrt{\frac{(\rho_2-\rho_1)(\mathrm{D}+\mathrm{h_1})\mathrm{h_1}(\mathrm{D}-\mathrm{h_1})\mathrm{g}}{\rho_1\mathrm{D}(2\mathrm{D}-\mathrm{h_1})}} \qquad (12)$$

Equation (12) can be normalized to get Eq. (13).

$$\frac{\mathrm{U_i}}{\sqrt{\mathrm{gD}}}=\sqrt{\frac{(\frac{1}{\gamma}-1)(1+\bar{\mathrm{h}})(1-\bar{\mathrm{h}})}{\frac{2}{\bar{\mathrm{h}}}-1}} \qquad (13)$$

Figure 3 presents the plot of Eq. (13) for γ=0.999. It is notable on the curve that from $\bar{h} = 0.5$ to almost 0.9, the normalized velocity is within 20% of the value at $\bar{h} = 0.5$, which is close to the measurement uncertainty of most flow visualization techniques. It is believed that this is the reason for observation of almost constant velocity for some durations after opening the gate valve.

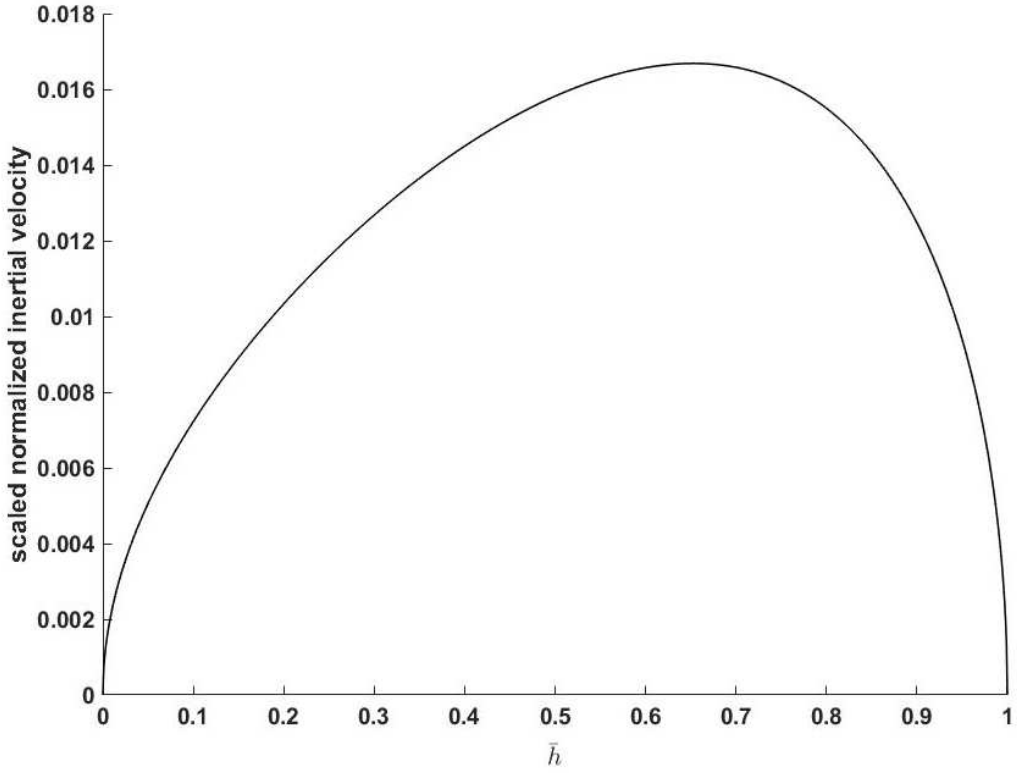


Figure 3. Normalized inertial front velocity for different values of normalized interface distance from the upper wall at position of the front for γ=0.999

This reasoning aligns with the classical argument originally proposed by von Kármán [21] and remains valid under the assumptions of hydrostatic pressure distribution and parallel flow. The thickness of the heavy fluid advancing into the lighter layer does not remain constant. Instead, it evolves in time due to the viscous redistribution occurring behind the front. The viscous region continuously supplies and reshapes the interface, thereby influencing the local front thickness. In this study, the inertial front velocity is taken to follow the form given in Eq. (13), while the temporal evolution of the front thickness is governed by the viscous flow dynamics. It was previously introduced in Yavari et al. [12].

Analytical Method and Solution Scheme to Determine Front Velocity

Although the governing equations of the viscous region are derived in closed analytical form, a numerical procedure is required to capture the time-dependent evolution of the front. This section outlines the analytical formulation and computational scheme used to evaluate the temporal progression of the advancing front.

Figure 4 presents the flow configuration immediately after the gate valve is opened. Point **P** denotes a representative location on the interface near the gate valve, where the viscous region is well described by the governing equations. Point **S** marks a location along the interface just upstream of the front bulge, beyond which the parallel-flow and viscous dominated assumptions are no longer valid. The region between **P** and **S** is treated as the domain over which the viscous equations determine interface evolution and thereby supply the conditions required to update the front thickness and its inertial velocity.

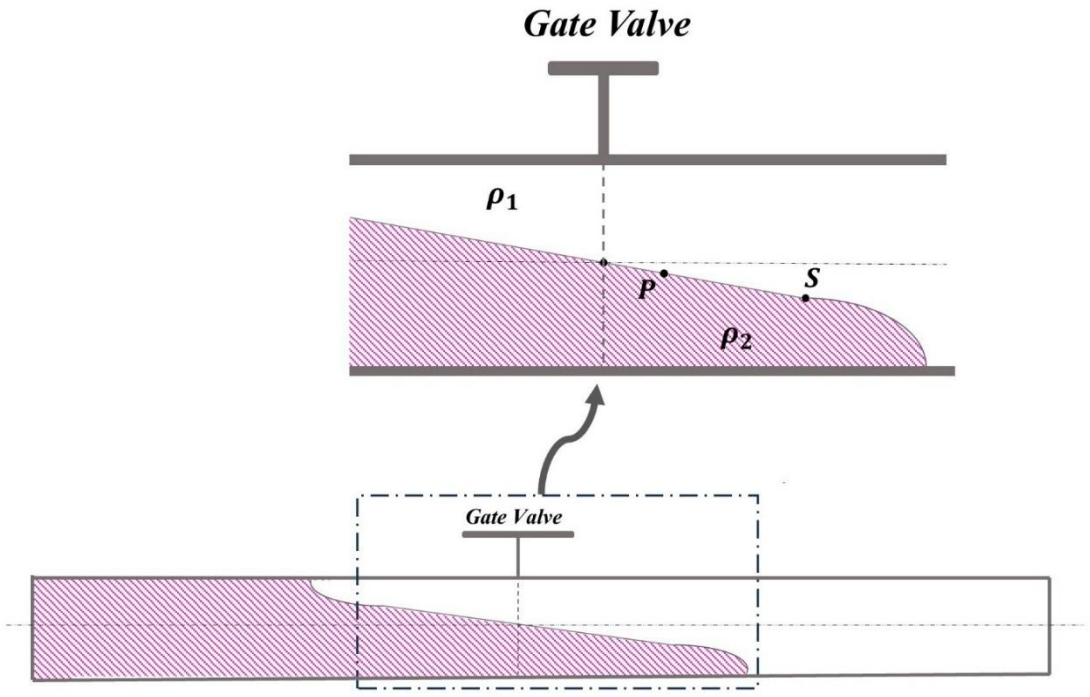


Fig. 4. Schematic of the flow after opening the gate valve

Upon removal of the gate, a symmetric bidirectional motion is initiated, with the flow initially appearing nearly parallel to the channel axis. Because the pressure gradient is stronger near the upper and lower walls, the local velocities in these regions are correspondingly higher. The initial discharge immediately after gate removal typically exceeds the flow rate predicted by Eq. (12). As the interface begins to flatten, the flow rate decreases, which in turn causes the interface to gradually tilt again relative to the horizontal. This adjustment may repeat in a weakly periodic manner. The overall discharge remains sufficiently large to generate transient mixing and local distortions of the interface. Farther downstream, the slope-driven viscous flow eventually adjusts to match the inertial flux associated with the prevailing front thickness, producing a quasi-steady equilibrium between the main flow and front. This equilibrium state is adopted as the initial condition for the numerical scheme developed in this study. A representative image of the flow field after equilibrium has been established is shown in Fig. 5.

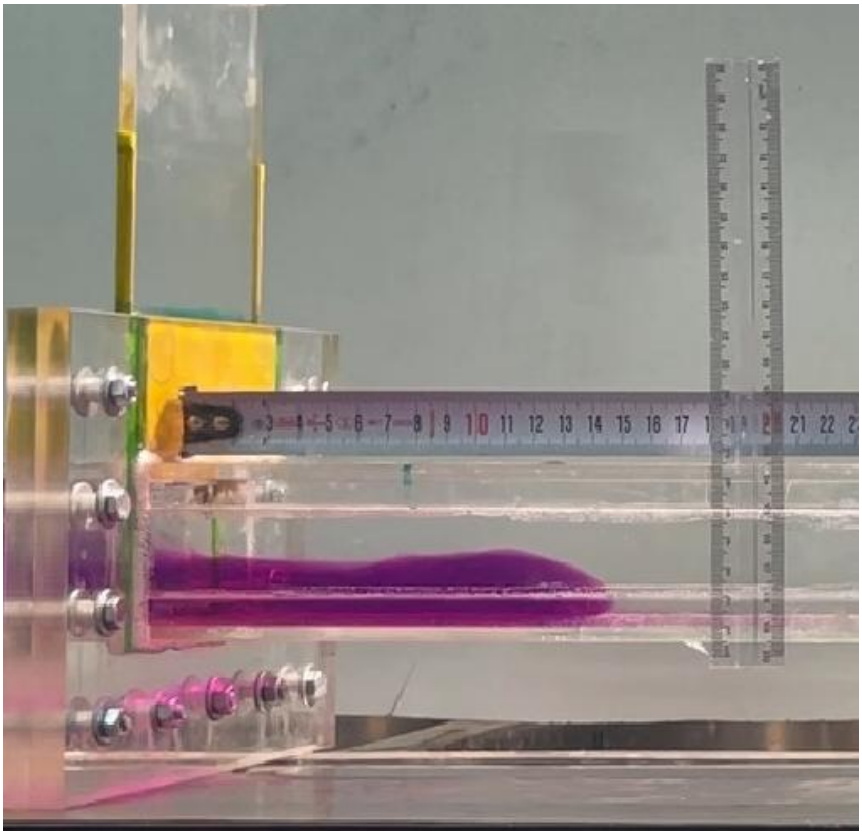


Figure 5. Front of heavy fluid after opening the gate valve, equilibrium for At=0.0006

To better understand the characteristics of equilibrium between the inertial and viscous flow, Eq. (14) presents a balance between the viscous and inertial flow rates based on Eq. (2) and Eq. (12).

$$\frac{(\rho_2-\rho_1)g\frac{\partial h_1}{\partial x}(D-h_1)^3}{12\mu}\left[\left(1-\frac{h_1}{D}\right)\left(1+\frac{h_1}{D}-\frac{2h_1^2}{D^2}\right)-1+\frac{3h_1}{D}\left(1+\frac{h_1}{D}-\frac{2h_1^2}{D^2}\right)-\frac{3h_1}{D}\right]$$
$$=\sqrt{\frac{(\rho_2-\rho_1)(D+h_1)h_1(D-h_1)g}{\rho_1 D(2D-h_1)}}(D-h_1) \qquad (14)$$

After normalizing the terms and canceling similar terms, Eq. (15) will be formed:

$$\frac{\sqrt{\rho_1(\rho_2-\rho_1)g}\frac{\partial h_1}{\partial x}D^{\frac{3}{2}}}{12\mu}(1-\bar{h})^2\left[(1-\bar{h})(1+\bar{h}-2\bar{h}^2)-1+3\bar{h}(1+\bar{h}-2\bar{h}^2)-3\bar{h}\right]$$
$$=\sqrt{\frac{(1+\bar{h})\bar{h}(1-\bar{h})}{(2-\bar{h})}} \qquad (15)$$

The terms in Eq. (15), excluding $\frac{\sqrt{\rho_1(\rho_2-\rho_1)g}\frac{\partial h_1}{\partial x}D^{\frac{3}{2}}}{12\mu}$ are drawn in Fig. 6. A coefficient has been used in place of $\frac{\sqrt{\rho_1(\rho_2-\rho_1)g}\frac{\partial h_1}{\partial x}D^{\frac{3}{2}}}{12\mu}$ to approach the curves to each other. It is clear that the curves representing the inertial and viscous flow rates collide near $\bar{h}$=0.6. If parameters are changed, the collision point will differ slightly but generally it occurs close to 0.6 as is demonstrated graphically in Fig. 6. The significance of the position of this point will be made clear later, as the effect of different parameters is assessed based on the evolution of the interface. The $\bar{h}$ coordinates of this point may be assumed almost constant for analysis in this study.

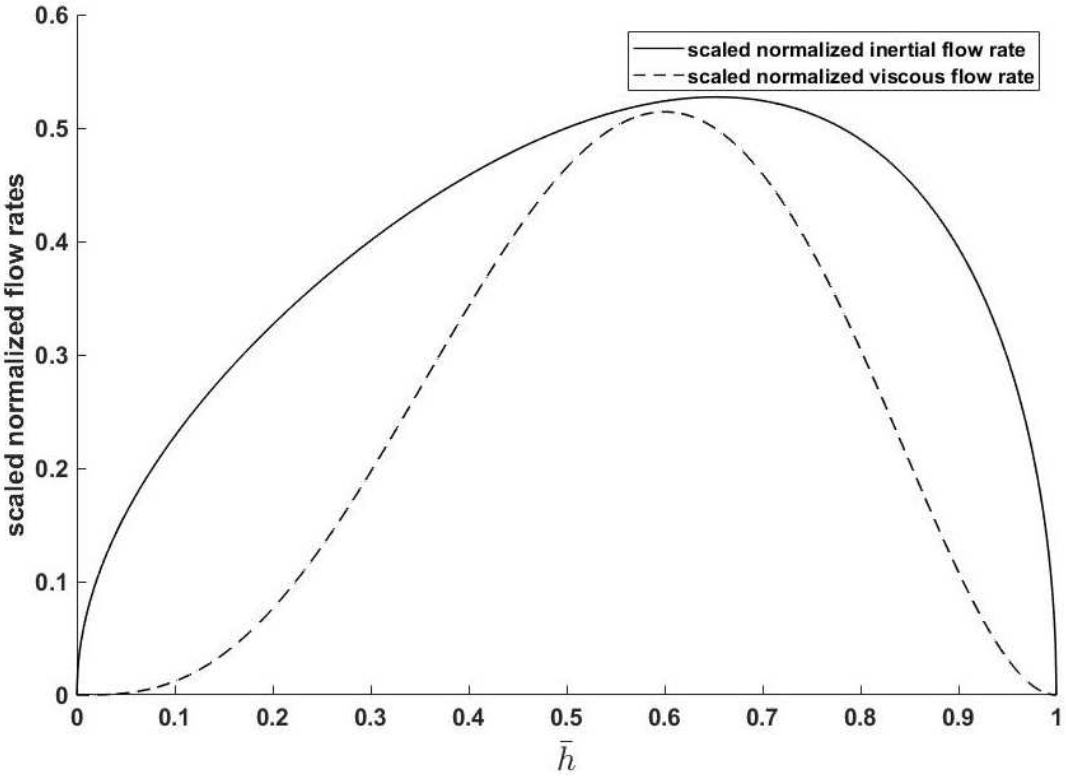


Fig. 6. Scaled inertial front flow and viscous flow rates

The aforementioned framework enables the determination of the front velocity using only the fundamental physics of the problem. The following procedure summarizes the algorithm employed in the analytical scheme for finding the evolution of the interface and front velocity.

1- Inititalization after equilibrium

Once the initial equilibrium is established, the gate valve position is taken as the origin. The interface slope at this instant is known from the preceding analysis. Owing to symmetry, the interface at the gate location is assumed to lie at mid-height. A reference point on the interface, denoted as P in Fig. 4, is selected immediately adjacent to the gate.

2- Tracking interface motion

By following the vertical displacement of point P (explained in 3)—which gradually rises toward the channel centerline—the temporal evolution of the interface slope at the gate can be determined. This, in turn, allows the heavy fluid flow rate at the gate to be updated continuously.

3- Computing interface rise

Using the initial estimate of the interface position, the upward motion of the interface (including point P) is computed at each time step. The rate of rise follows directly from the governing expression for interface evolution, Eq. (16) which is a reformulation of Eqs. (4) and (5). Equation (16) is written in terms of the normalized thickness $\bar{h} = \frac{h_1}{D}$:

$$\frac{\partial h_1}{\partial t} = \frac{-(\rho_2 - \rho_1)D^2 g(\frac{\partial h_1}{\partial x})^2(1-\bar{h})^2}{12\mu}\left[\left(1+\bar{h}-2\bar{h}^2\right)\left(-1-8\bar{h}\right)+\left(1-\bar{h}\right)\left(-2-2\bar{h}-8\bar{h}^2\right)\right.$$
$$\left.+3+9\bar{h}\right] \qquad (16)$$

The above equation for the rate of change of h_1 is in accordance to the convention in Yavari et al. [18]. It means that Eq. (16) is negative for $\bar{h} > 0.5$ which indicates a rising level of heavier fluid after opening the gate valve, in the lighter fluid side. Equation (16) is plotted in Fig. 7 for different values of interface slope. The interface slope is also determined by the simple equation below for every point on the interface.

$$Interface\ slope = \frac{h_{1_i} - h_{1_{i+1}}}{\Delta x} \qquad (17)$$

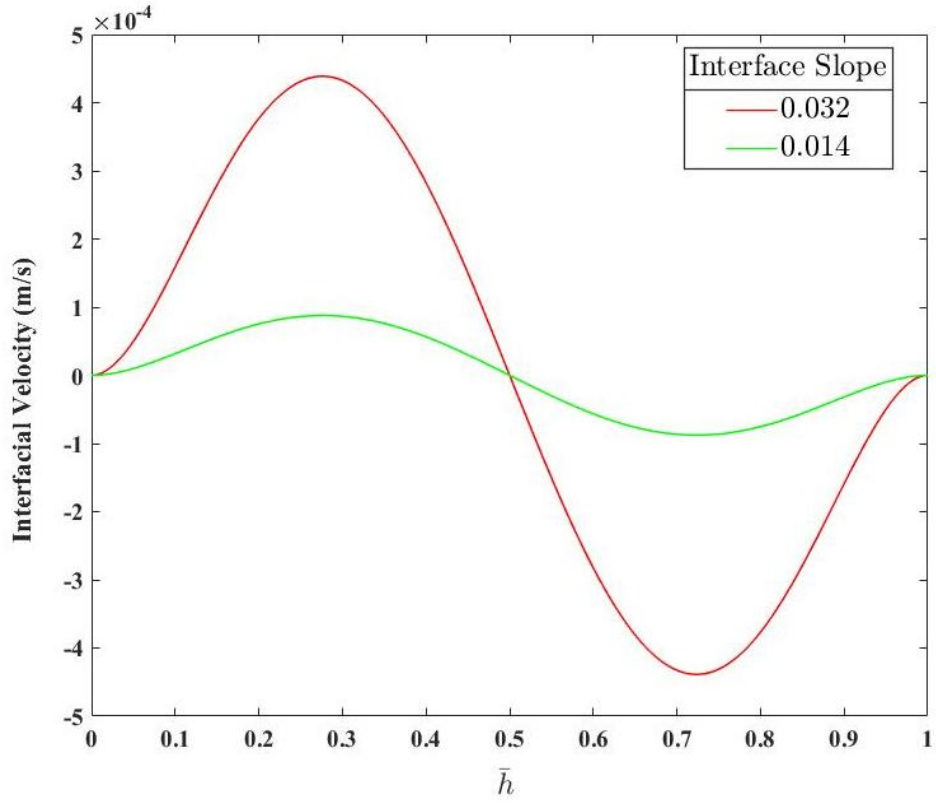


Fig. 7. Plots of Eq. (16) for different values of interface slopes. The curves have been plotted using $\rho_2 = 1001\ \mathrm{kg/m^3}$, $\rho_1 = 1000\ \mathrm{kg/m^3}$, μ=0.001 $\mathrm{N.S/m^2}$ and D=0.05 m to get quantitative values on the ordinate axis

4- Calculation of heavy fluid flow rate at gate valve

The flow rate of the heavy fluid at gate valve is calculated over time. As was noted it is possible to pick point P at the vicinity of the gate valve, located on the interface and follow its movement by using Eq. (18).

$$h_{1_{P_2}} = h_{1_{P_1}} + \left.\frac{\partial h_1}{\partial t}\right|_{@h_{1_{P_1}}} \Delta t \qquad (18)$$

Based on convention and Eq. (16), it indicates a rising interface and a decreasing interface slope. The flow rate at position of the gate valve can be calculated by considering Eq. (2) and is given by Eq. (19). In the following equations i indicates the axial steps and t_i is the time step.

$$Q_2(t_i) = \frac{(\rho_2 - \rho_1) g \left(\frac{D}{2}\right)^3 \frac{\partial h_1}{\partial x}}{12\mu} \left(-\frac{1}{2}\right) \qquad (19)$$

5- Finding the volume rise associated with rise of interface level

It is possible to calculate the volume increase associated with increasing the interface level as the interface is moving upward towards the channel centerline:

$$V_{inc,total} = \sum_{i=2}^{\left\lfloor \frac{X_f}{\Delta x} \right\rfloor} \frac{h_{1_{i,1}} - h_{1_{i,2}} + h_{1_{i-1,1}} - h_{1_{i-1,2}}}{2} \times \Delta x \qquad (20)$$

This scheme will lead to a nonlinear evolution of the interface based on the dynamics of the flow and interface evolution defined by previous equations.

6- Calculating the flow responsible for advancing the front

The heavy fluid flow rate at the gate valve can be conceptually divided into two components. The first component is expended in raising the interface between the gate and the onset of the frontal bulge. The second component drives the front itself forward. This front-propagating portion of the flow is expressed through the following relationship:

$$V_{surplus} = Q_2 \Delta t - V_{inc,total} \qquad (21)$$

Dividing the volume by the time interval it is possible to get the flow rate which advances the front as:

$$Q_{surplus} = \frac{V_{surplus}}{\Delta t} \qquad (22)$$

The value of Eq. (22) represents the flow rate of the front which advances the flow. By finding the flow rate of the front it is possible to estimate the front thickness for the next time step based on Eq. (23)

$$h_{1f}(i+1) = h_1 \quad \text{at which } Q_{if} = Q_{surplus}(i+1) \qquad (23)$$

and new position of the front:

$$X_f(i+1) = X_f(i) + U_i(i+1)\Delta t \qquad (24)$$

U_i was given in Eq. (12) and subscript f in above equations denotes that the parameters relate to the front not behind that.

7- Continuation of the algorithm

If the frontal displacement during the given time step does not exceed the next axial grid interval, the algorithm is simply repeated to update both the interface position and the corresponding front velocity. However, if the front advances far enough to cross into the next axial step, the interface must be extended to accommodate this forward movement. Physically, the front flow must equal the viscous flux feeding it from behind. Therefore, Eq. (2) is applied using the value of h_1 at the last resolved point on the interface to determine the local interface slope. The interface is then extrapolated linearly over the distance traversed by the front. This extension is performed using Eq. (25), which provides the appropriate linear continuation of the interface geometry.

$$h_{1_{i,2}} = h_{1\left\lfloor\frac{X_{f,t_{i-1}}}{\Delta x}\right\rfloor,2} - \left(\frac{\partial h_1}{\partial x}\right)_{\left\lfloor\frac{X_{f,t_{i-1}}}{\Delta x}\right\rfloor} . \Delta x . \left(i - \left\lfloor\frac{X_{f,t_{i-1}}}{\Delta x}\right\rfloor\right) \qquad (25)$$

There is an important point in this algorithm which should be clarified before presenting the results. The value of h_{1f} calculated in Eq. (23) varies considerably with the value of $h_{1\left\lfloor\frac{X_{f,t_i}}{\Delta x}\right\rfloor,2}$ or $h_{1\left\lfloor\frac{X_{f,t_{i-1}}}{\Delta x}\right\rfloor,2}$ (or any points between them) which are the most forward points in Eq. (25) or the last points of the interface. In other words, the interface thickness observed immediately behind the front—clearly identifiable in the experiments—is not the same as the front thickness defined in Fig. 2. This distinction can easily lead to ambiguity. The underlying reason is that the physical mechanisms governing the interface region differ fundamentally from those acting at the front itself. For example, previous investigations such as Ref. [24] have reported a localized downward motion near the leading edge, indicating that complex secondary motions may arise in the frontal zone. Although that specific observation does not directly apply to the present configuration, it highlights that the flow near the front can deviate substantially from the parallel-flow dynamics governing the bulk interface. Further discussion of this issue is provided later. This step in the algorithm is a major resolving point in relating the main flow to the front flow.

Before examining the variations in the interface thickness behind the front, it is essential to distinguish between two different quantities as introduced before:

(i) The front thickness, which corresponds to the inertial thickness discussed in Step 6 of the algorithm, and

(ii) The interface thickness immediately behind the front, which corresponds to the terminal segment of the viscous interface and was analyzed in Step 7.

These two thicknesses arise from different physical mechanisms—the inertial front thickness from the local pressure-driven dynamics, and the interface thickness behind the front from the viscous evolution of the interface—and therefore need not coincide. Understanding this distinction is key to interpreting the results presented later.

Results and discussion

In this section, the results obtained from the analytical scheme are presented. These results are then compared with selected experiments from Ref. [14] as well as additional measurements conducted by the authors. Finally, a set of physical interpretations is provided to discuss the interface evolution inferred from the analytical predictions.

Flow rates and front velocity for preliminary validation

To estimate the overall reliability of the analysis, Fig. 8 shows the analytically computed front velocity and experimental front velocity during the first 90 seconds following equilibrium for several values of the heavy fluid density. All cases employ a lighter fluid density of 1011.3 kg/m^3, representative of the water used for experiments. Over the plotted time interval, the front velocity exhibits only a very slight decay, appearing nearly constant which is consistent with the behavior typically observed in the relatively short experimental setup introduced later.

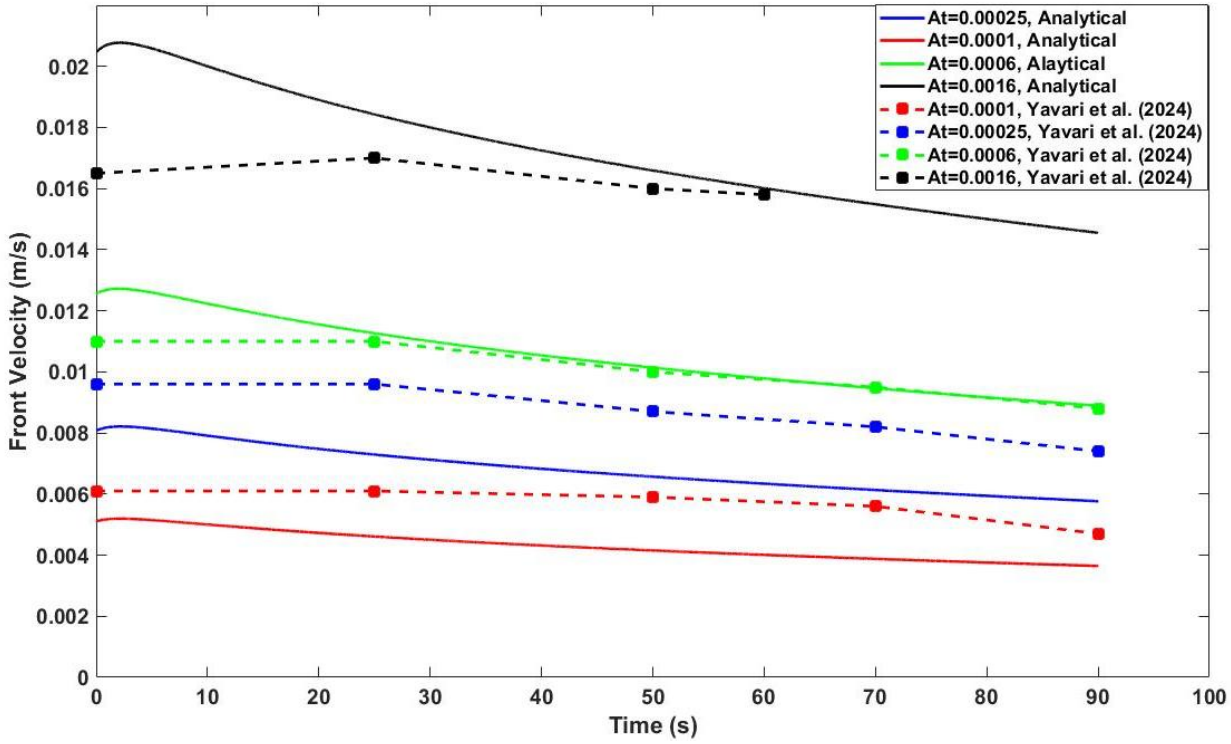


Fig. 8. Variations of front velocity for different values of density of the heavy fluid. In all plots, $\rho_1 = 1011.3\ \mathrm{kg/m^3}$, μ=0.001 $\mathrm{N.S/m^2}$ and D=0.05 m. The experimental data are from Yavari et al. (2024)

As seen in Fig. 8, the experimental measurements agree well with the analytical predictions developed in this study, with most data falling within approximately 15% of the analytical values. This level of agreement is promising considering the fact that the experimental uncertainties are about 5% in the measured front velocity and roughly 11% in the Atwood number. Immediately after gate removal, especially at higher density contrasts, mixing and small-scale turbulence further complicate accurate measurement of the instantaneous front velocity. Another clear trend in Fig. 8 is that, for larger Atwood numbers, the experimental front velocity tends to fall below the analytical prediction. This is expected, as even in horizontal configurations increased density contrast promotes localized mixing and interfacial disturbances that reduce the effective density difference driving the front.

The proposed analytical framework partitions the heavy fluid flow at the gate into two components: one that elevates the interface behind the front and another that drives the front forward. Figure 9 illustrates this decomposition by showing how the total heavy fluid discharge is divided into these two contributions.

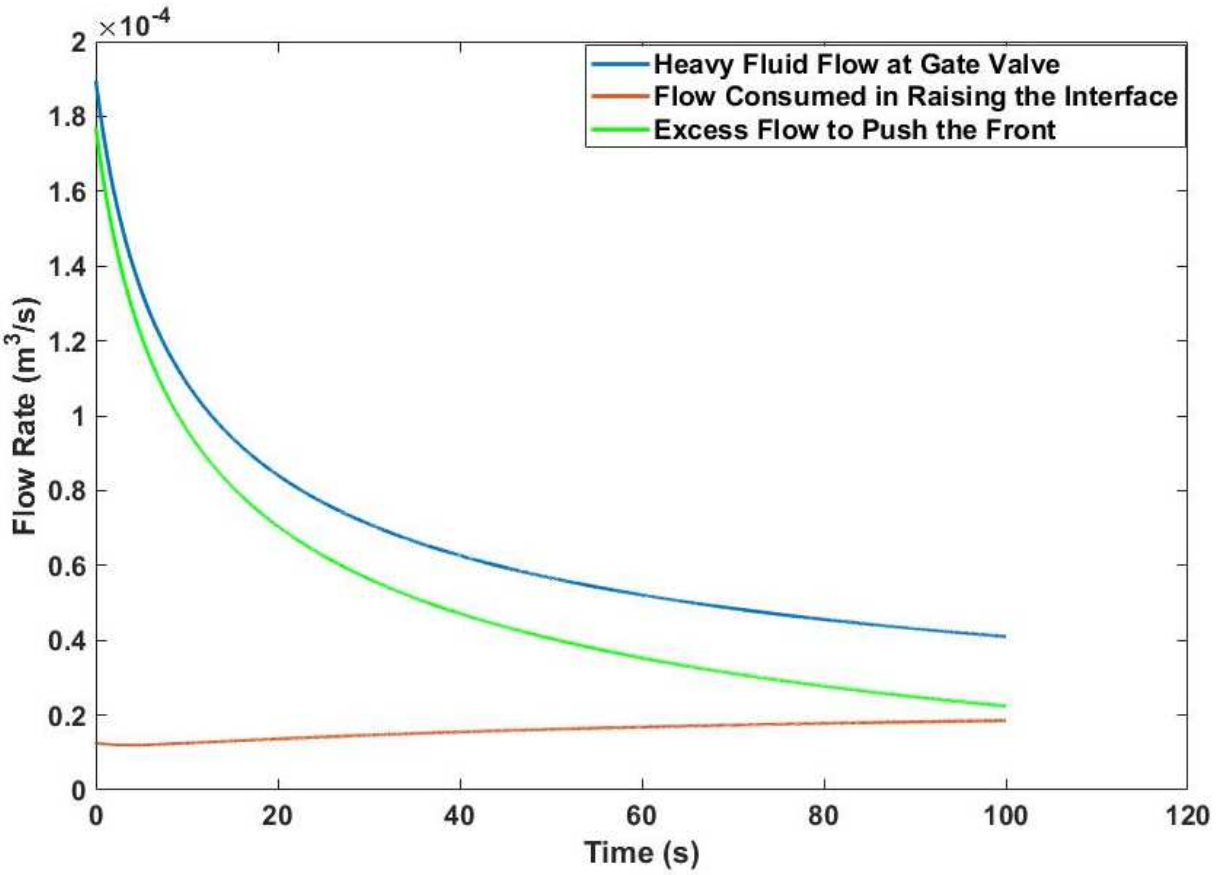


Fig. 9. Heavy fluid flow rate at position of the gate valve, divided into one part increasing the interface level (red curve) and another for pushing the front (green curve) for At=0.00025.

The blue curve in Fig. 9 shows that the total heavy-fluid discharge at the gate decreases as the interface slope gradually relaxes there. The red curve represents the portion of discharge corresponding to the raise of the interface downstream, while the remaining portion—shown in green—corresponds to the flow that drives the front forward. The steady decline of the green curve indicates a reduction in the propulsive flow available to the front, consistent with the observed gradual decrease in front velocity and with the underlying physics of the system.

To further illustrate the predictive capability of the proposed analytical model, Fig. 10 presents the front position as a function of time from the equilibrium state for several Atwood numbers. The overall agreement across the tested range demonstrates the robustness of the model in capturing the essential dynamics of gravity currents and their front propagation. At higher density contrasts, early-stage mixing and interfacial instabilities introduce minor deviations from the idealized analytical predictions.

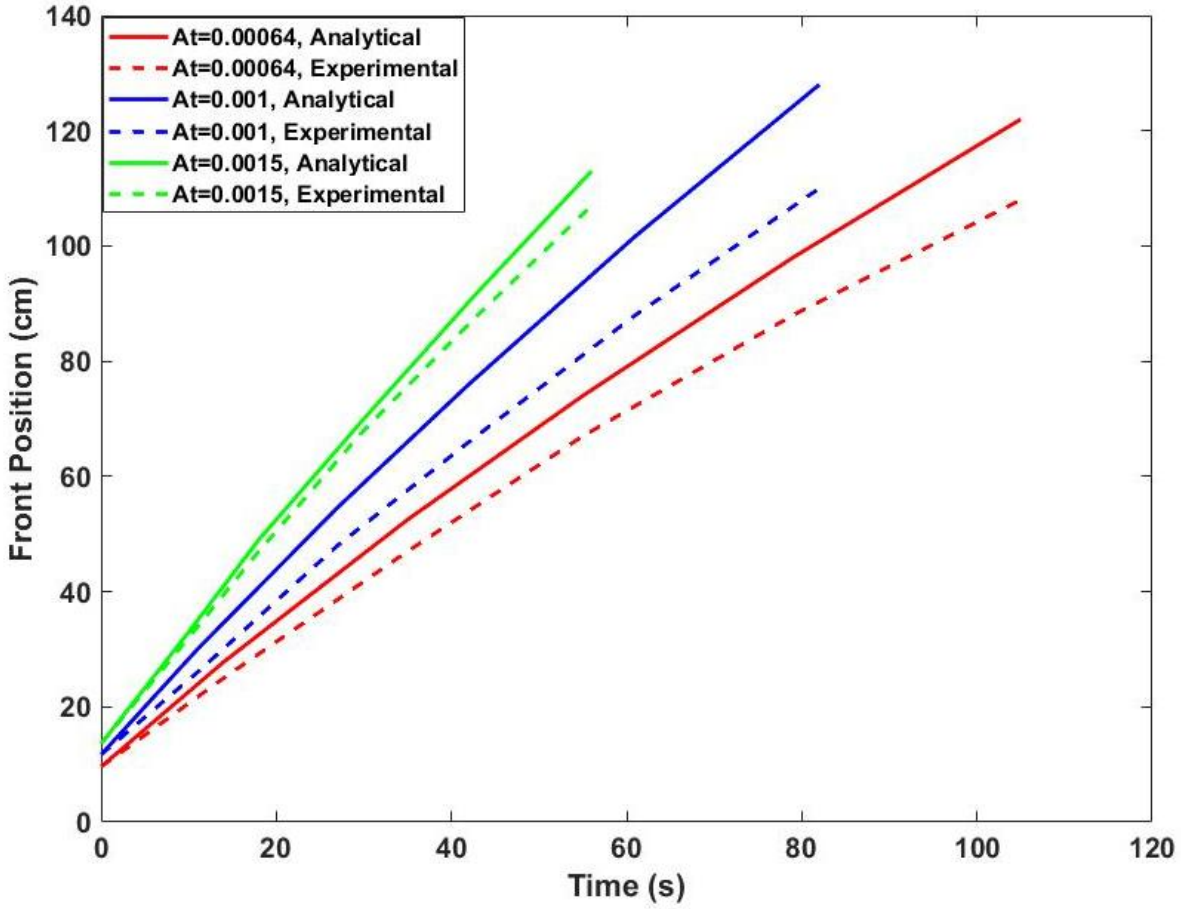


Fig. 10- Front position versus time for selected Atwood numbers in experiments compared to the results from the analytical model

Front Characteristics

One of the most important parameters in lock-exchange flows or gravity currents is the front dynamics. Two important parameters are affecting the front namely thickness behind the front and inertial front thickness. The thickness behind the front can easily be measured using the experiments employed in this study. The inertial front thickness requires detailed knowledge of flow within the head of the current and needs rigorous Direct Numerical Simulation (DNS) or very accurate Particle Image Velocimetry (PIV) to be detected.

In Fig. 11 the interface thickness behind the front estimated by the analytical method is compared against the experiments. As observed, the results are in reasonable agreement which underscore the ability of this model to predict the thickness behind the front, a major parameter in this class

of flow. The minor deviations of the analytical results from the experiments are within the experimental uncertainties and are affected by the mixing of the fluids.

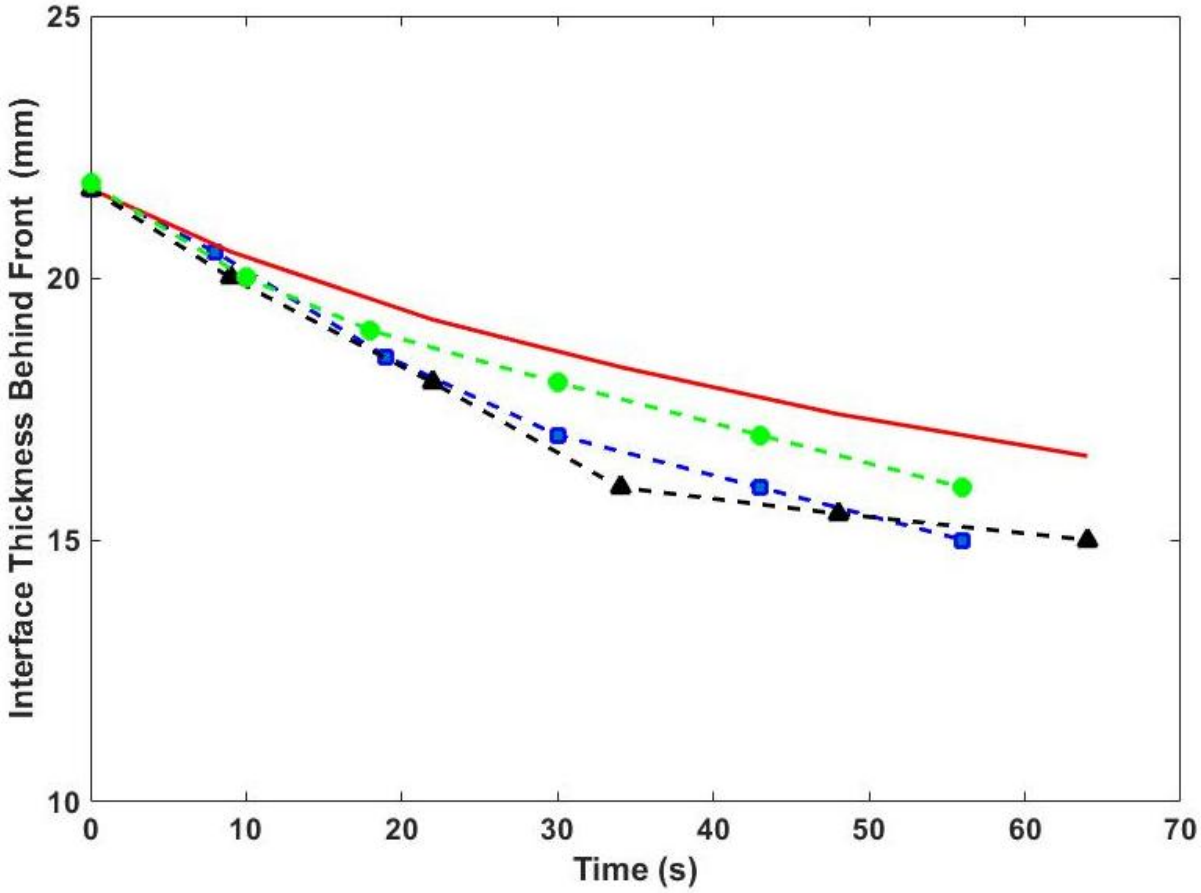


Fig. 11- Variations of thickness behind the front in horizontal lock-exchange flow. Solid red curve represents analytical results. The dashed curves are experimental results. At= 0.002●, At= 0.0017■, At=0.0013▲

An important and somewhat unexpected observation arises from Fig. 11. As noted in the caption, although three different Atwood numbers are shown experimentally, only a single analytical curve is plotted. This is because the analytically predicted interface thickness behind the front is inherently independent of the density contrast between the fluids. While this may initially appear counterintuitive, the underlying reasoning will be clarified later in this article.

Figure 12 represents the timely evolution of the front thickness and interface thickness behind the front for comparison for a representative case of low Atwood number flow.

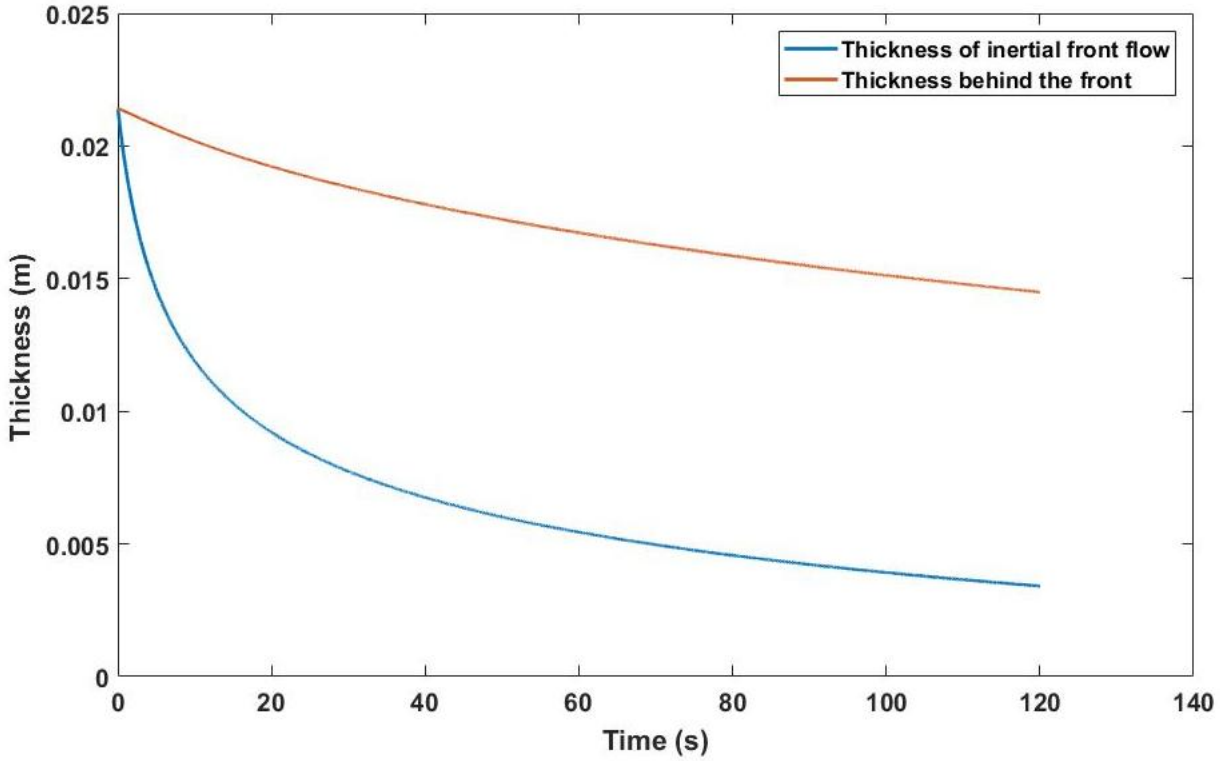


Fig. 12- Variations of inertial front thickness and the thickness behind the front in horizontal channel. At= 0.0005, D=0.05 m and μ=0.001 $N.S/m^2$

To better illustrate the evolution of the interface—and specifically the interface thickness immediately behind the front—Fig. 13 is presented. Each curve corresponds to the interface profile at 10-second intervals. The final point on each curve represents the terminal point of the interface just upstream of the front. Therefore its value corresponds to the "interface thickness behind the front". This visualization highlights how the interface progressively reshapes as the viscous region evolves over time.

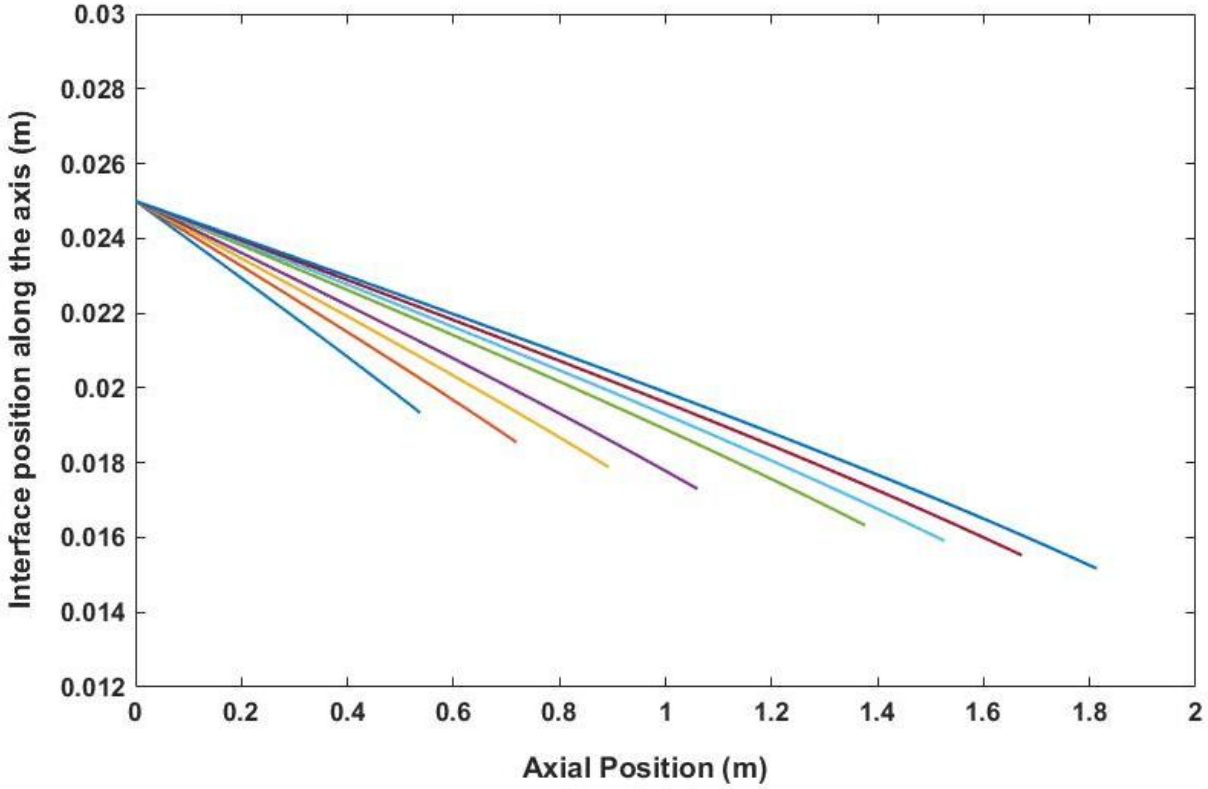


Fig. 13. Evolution of the interface at 10 second intervals, At= 0.0015, D=0.05 m and μ=0.001 $N.S/m^2$

In the following sections, these observations—along with the underlying mechanisms responsible for them—are examined in greater detail.

Experiments

To validate the analytical results, selected experimental data—previously reported in detail in Refs. [14] and [25], including their associated uncertainties—were incorporated into the preceding figures. Only a brief overview of the experimental procedure and relevant qualitative observations is provided here, as the full methodology has already been thoroughly documented.

Experimental setup

The experiments were conducted in a straight, transparent rectangular channel divided into two equal sections by a sliding gate valve. The channel is 2.4 m long and has an internal height of 5 cm, width of 10 cm, and wall thickness of 0.5 cm. Two ports with 12.5 mm diameter are located near each end for filling and drainage. As noted earlier, these experiments were not designed specifically for the present study, and the channel length is shorter than ideal for full validation of the analytical scheme. Nevertheless, reliable comparisons can still be made for short time intervals following gate removal. Based on the uncertainty analysis reported in Refs. [14] and [25], the front velocity measurements carry an estimated error of approximately 5%, while the front thickness measurements show an uncertainty of about 4% under conditions of a stable interface. The Atwood number exhibits a larger uncertainty, exceeding 11%. A three-dimensional rendering of the experimental setup is shown in Fig. 14.

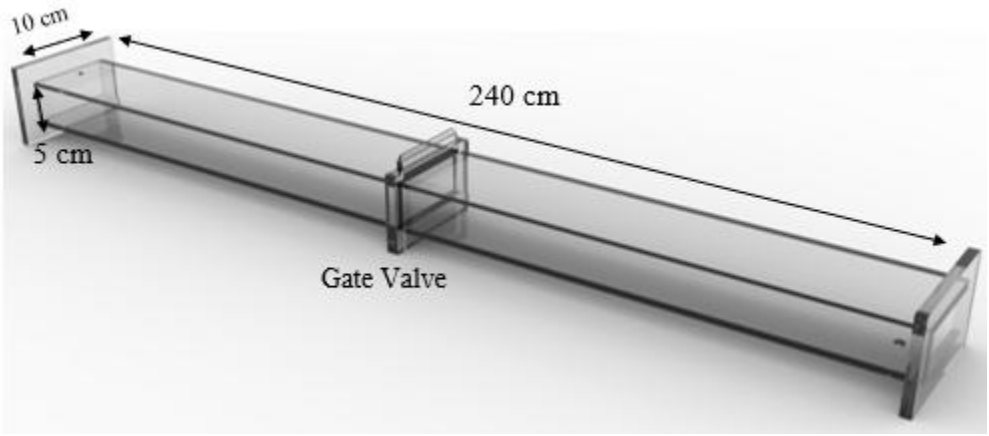


FIG. 14. Three-dimensional model of the experimental setup

Qualitative observations

The analytical scheme begins at the moment when the flow reaches its initial equilibrium state, illustrated in Fig. 5. This equilibrium is defined as the earliest time at which the interface becomes clearly identifiable and the transient turbulence generated immediately after gate removal has subsided. Figure 15 compares the flow field just before equilibrium with that at the equilibrium moment. In Fig. 15(a), the flow rate is visibly greater than what the front can accommodate, resulting in a distorted interface. In contrast, Fig. 15(b) shows a straight, undisturbed interface,

indicating that the excessive initial discharge has diminished and the system has reached the equilibrium condition used to initiate the analytical procedure.

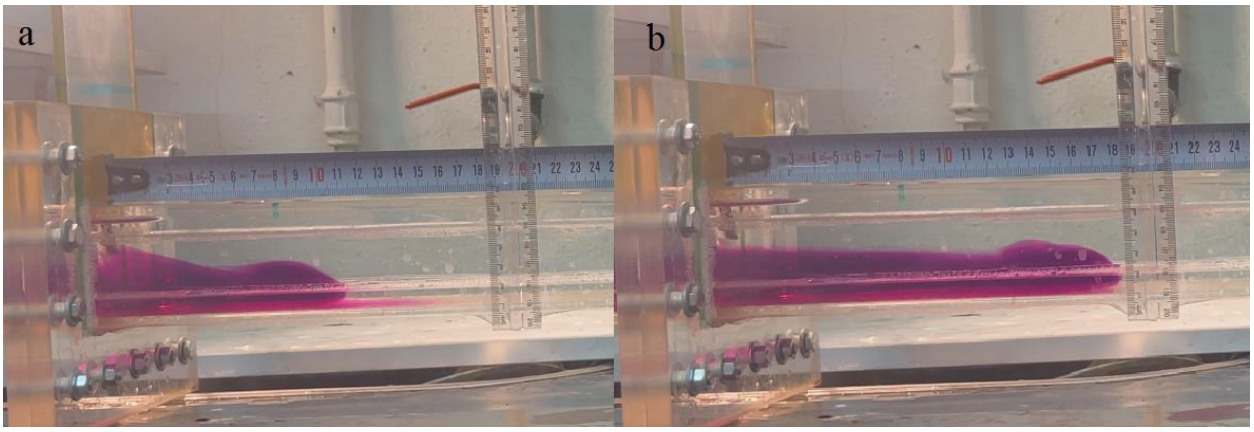


Fig. 15. Flow after opening the gate valve for an experiment. a) before equilibrium b) after equilibrium

Another qualitative observation from the experiments concerns the interface thickness behind the front. In the discussion of Fig. 11, it was noted that the analytical prediction for the evolution of this thickness is represented by a single curve, independent of the Atwood number. To illustrate this behavior experimentally, Fig. 16 presents four representative snapshots. The top two show the flow 40 seconds after equilibrium for Atwood numbers of 0.0006 and 0.00035, while the bottom two show the flow 15 seconds after equilibrium for Atwood numbers of 0.0045 and 0.01. Despite the substantial differences in density contrast, the interface thickness immediately behind the front is nearly identical for equal times after equilibrium. This consistent behavior across a wide range of Atwood numbers supports the analytical prediction shown in Fig. 11 and reinforces the conclusion that the post-front interface thickness evolves independently of the density contrast.

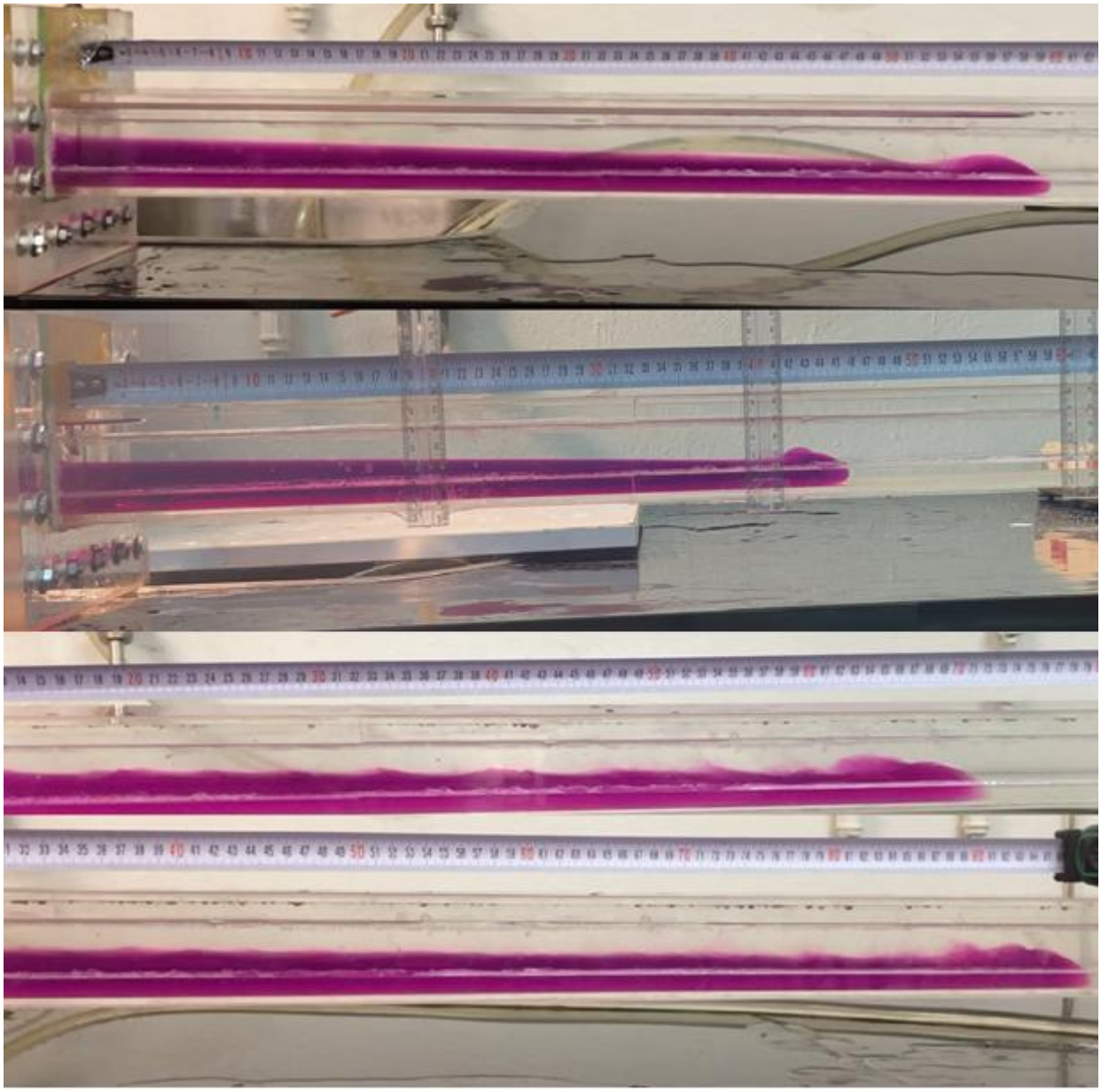


Fig. 16. Snapshots of the flow at different Atwood numbers. The top two snapshots represent At=0.0006 and At=0.00035 respectively, 40 seconds after equilibrium. The bottom two present At=0.0045 and At=0.01, 15 seconds after equilibrium.

As it is observed in the snapshots, the axial positions of the fronts are different at equal times which is because of the fact that the fronts with different density contrasts move at different velocities. In addition, the position of initial equilibrium is different for different Atwood numbers. The small difference in form or thickness of the front may be attributed to experimental errors or other discrepancies in calculation of time or equilibrium distance as well as mixing of fluids.

Effect of different parameters on dynamics of the flow

In this section, the influence of various flow parameters on the overall dynamics is examined analytically. Verifying some of these effects experimentally would require additional dedicated setups—for instance, channels with modified dimensions or geometries. Moreover, each setup must be sufficiently long to allow accurate observation of the flow over extended periods after the gate valve is opened. As such, the present analysis focuses primarily on theoretical predictions,

Effect of density contrast

To evaluate how variations in the system parameters influence the subsequent flow dynamics, it is first necessary to understand how these changes modify the equilibrium state established immediately after the gate is opened. As discussed earlier, the initial equilibrium configuration determines both the local interface slope and the discharge rate of the heavy fluid at the gate valve. These, in turn, set the initial front thickness and the characteristic equilibrium length—the distance from the gate at which the inertial front motion becomes fully compatible with the viscous flow behind it. Any alteration to the channel geometry, fluid properties, or external forcing will therefore manifest first through changes in this equilibrium state. It then propagate into the long-term evolution of the interface and front velocity. Equation (26) shows the equilibrium length by balancing the viscous and inertial flow rate after opening the gate valve.

$$X_{f,eq} = \frac{\sqrt{\rho_1(\rho_2-\rho_1)g}D^{\frac{5}{2}}}{12\mu}\left(\frac{1}{2}-\bar{h}_{eq}\right)\left(1-\bar{h}_{eq}\right)^2\left[\left(1-\bar{h}_{eq}\right)\left(1+\bar{h}_{eq}-2\bar{h}_{eq}{}^2\right)-1 + 3\bar{h}_{eq}\left(1+\bar{h}_{eq}-2\bar{h}_{eq}{}^2\right)-3\bar{h}_{eq}\right]\sqrt{\frac{\left(2-\bar{h}_{eq}\right)}{\left(1+\bar{h}_{eq}\right)\bar{h}_{eq}\left(1-\bar{h}_{eq}\right)}} \qquad (26)$$

In Eq. (26), $\bar{h}_{eq}$ corresponds to the equilibrium position (almost equal to 0.6) and has no dimension. It means that $\frac{\partial h_1}{\partial x}$ may be proportional to $\frac{1}{\sqrt{\rho_1(\rho_2-\rho_1)g}}$ for equilibrium. Furthermore, if the interface thickness at the equilibrium location remains approximately constant, then the equilibrium front position must scale with the inverse square root of the density contrast. For example, if the density contrast is increased by a factor of four, the resulting equilibrium length will increase by a factor of two. This scaling arises directly from the balance between inertial front motion and the viscous

flow supplied from behind the front, which requires a longer distance for stronger buoyancy forces to establish the same equilibrium interface geometry. Then based on $Q_2(i)$ in Eq. (18), the heavy fluid flow rate at position of the gate valve is proportional to $\sqrt{\rho_2 - \rho_1}$ for the first time step. It means that if density contrast in increased by a factor of four, the initial flow rate of heavy fluid at position of the gate valve is increased by a factor of two.

So based on $\frac{\partial h_1}{\partial t}$ in Eq. (16), the rate of change of front thickness is independent of density contrast, within the first time-step for similar values of $\bar{h}$ as the density contrast is multiplied by the square of interface slope. Therefore, the volume increase due to the rise in interface level is proportional to $\sqrt{\rho_2 - \rho_1}$ because of the proportionality of equilibrium length in the first time step and also assumption of a linear interface at equilibrium.

One important point deserves clarification. At the first time step, the heavy fluid discharge at the gate is proportional to the square root of the density difference. After that initial impulse, however, the local interface slope at the gate is updated according to Eq. (16). If the slope at the gate is reduced to half its previous value, the reference location P_1 used to compute the slope moves to halfway between the centerline and the previous point on the curve in Fig. 7. Because the interface profile in the vicinity of the center is nearly linear, the vertical motion of P_1 will be roughly half the previous rate. Consequently, using the expression for Q_2 , the gate discharge remains proportional to $\sqrt{\rho_2 - \rho_1}$ (i.e., two times the base value in the example), while its instantaneous rate of change is reduced in proportion to the smaller slope.

At later time steps, it is essential to determine whether the increase in fluid volume behind the front continues to scale with $\sqrt{\rho_2 - \rho_1}$. Consider a representative point on the interface—such as the midpoint between the gate valve and the front. As previously discussed, for the first time step, this point and its immediate neighbor rise at a rate that is effectively independent of the density contrast. After the front advances and the interface reshapes, the same two points remain close to the midpoint, and because the interface is nearly linear over this region (as seen in Fig. 7), their relative upward displacements remain essentially unchanged.

To illustrate, suppose the density contrast increases by a factor of nine. In the baseline case, the midpoint rises by one unit and the adjacent point by approximately (1+f), where (f) is a small

fraction. When the density contrast is increased, both points still rise by the same respective amounts (1 and (1+f)), so the local slope between them (which is one third of base condition)—and therefore the local interface angle—remains unchanged. Because the interface evolves at the same geometric rate regardless of density contrast, the volume increase associated with interface rise scales only with the horizontal extent of the interface. Since the equilibrium front position scales as $\sqrt{\rho_2 - \rho_1}$, the total volume increase likewise scales with $\sqrt{\rho_2 - \rho_1}$. Given that the heavy fluid discharge at the gate $Q_2(i)$ also scales with $\sqrt{\rho_2 - \rho_1}$, the resulting surplus flow is given as:

$$Q_{Surplus} = Q_2(i) - Q_{Interface} \qquad (27)$$

The value of Eq. (27) must inherit the same proportionality. Since the inertial front flux must equal this surplus flow, it follows directly—consistent with Eq. (28)—that the front flow rate and front velocity scale with $\sqrt{\rho_2 - \rho_1}$.

$$Q_{inertial} = D^{\frac{3}{2}} \sqrt{\frac{(\rho_2 - \rho_1)(1 + \hat{h})\hat{h}(1 - \hat{h})g}{\rho_1(2 - \hat{h})}}(1 - \hat{h}) \qquad (28)$$

It follows that the inertial front flow is likewise proportional to $\sqrt{\rho_2 - \rho_1}$. Consequently, for a fixed time increment Δt, the evolution of the front thickness—controlled by the surplus viscous discharge feeding the front—proceeds at the same rate regardless of the density contrast between the two fluids. In other words, while the amount of fluid arriving at the front scales with $\sqrt{\rho_2 - \rho_1}$, the geometric evolution of the front thickness does not. That is because both the viscous contribution and the required inertial front flux scale identically with the density difference.

However, although the temporal evolution of front thickness is density-independent, the associated front velocity is not. As shown previously in Eq. (12), the inertial front velocity depends explicitly on the reduced gravity $g' = g\frac{\rho_2 - \rho_1}{\rho_2}$ and therefore increases with increasing the density contrast. Thus, the fronts of flows with different density contrasts thicken in the same manner over time, but they advance at different speeds.

Another important parameter is the interface thickness behind the front. As previously discussed, whenever the front advances by one axial increment in the analytical scheme, the interface slope

at the previous station is updated. This refinement ensures that the viscous flow predicted by Eq. (2) matches the excess flow that leaves the interface and feeds the front—a physically consistent requirement. In this way, the interface evolves naturally within the model.

Earlier, it was shown that the inertial front flow is proportional to $\sqrt{(\rho_2-\rho_1)}$. From the initial time steps onward, this front flow is coupled with the local thickness behind the front to determine the interface slope. Because the slope adjusts at each step to satisfy mass continuity, it tends to maintain a proportionality of approximately $1/\sqrt{(\rho_1(\rho_2-\rho_1)g)}$. Through Eq. (2), this implies that the viscous flow rate behind the front also scales with $\sqrt{(\rho_2-\rho_1)}$. Since both the viscous contribution and the inertial front flow share this same proportional dependence, their ratio remains constant in time. Consequently, the thickness behind the front must evolve identically for equal elapsed times, regardless of density contrast, in order to preserve this proportionality. Based on the previous discussion proposition 1 and 2 of this study are stated as below:

Proposition 1. Distinct physical meanings of front thickness and interface thickness behind the front

"In horizontal lock-exchange flows, the thickness of the advancing front and the thickness of the interface immediately behind the front are governed by fundamentally different physical mechanisms and are distinct quantities. While the front thickness is determined by inertial momentum balance at the leading edge, the thickness behind the front is controlled by viscous redistribution in the upstream flow. "

Proposition 2. Independence of front and post-front thicknesses from density contrast

"In horizontal lock-exchange flows under the assumptions of parallel flow, negligible mixing, and weakly non-Boussinesq conditions, the temporal evolution of the interface thickness behind the front and thickness of the advancing front are independent of the density contrast between the fluids."

A recurring and robust outcome of the present analytical scheme is that the thickness of the heavy-fluid layer immediately behind the advancing front converges to a nearly constant fraction of the channel height. Across all analysis performed for horizontal two-dimensional configurations, this thickness approaches approximately 0.2D, where D is the channel height, regardless of the density contrast between the two fluids. This convergence is not imposed a priori, nor does it result from

a geometric constraint or symmetry argument. Instead, it emerges naturally from the coupling between the viscous redistribution of fluid behind the front and the inertial dynamics governing the front motion itself. As the interface evolves, the viscous flow supplied from the main body of the current adjusts continuously to match the inertial flux required to sustain the advancing front. This compatibility condition selects a unique and stable interface thickness behind the front, to which the system relaxes over time. Figure 17 depicts the evolution of the interface thickness behind the front (independent of density contrast) for three channel heights.

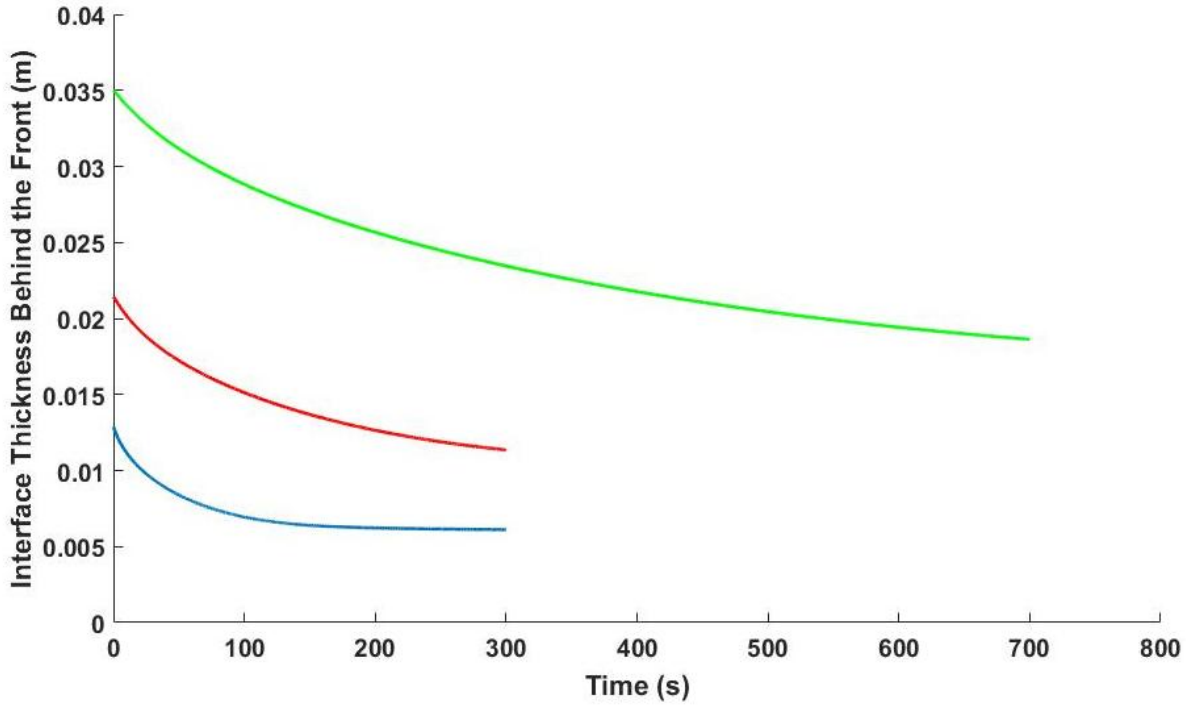


Fig. 17. Interface thickness behind the front versus time for three different channel heights. D=0.03m (-), D=0.05 m (-), D=0.08 m (-), the curves approach asymptotically to 0.2D for all values of channel's height

It is possible to introduce proposition 3 of this study as follows.

Proposition 3. Asymptotic selection of interface thickness behind the front

"In horizontal two-dimensional lock-exchange flow, the thickness of the heavy-fluid layer immediately behind the advancing front asymptotically converges to a fixed fraction of the channel height. This asymptotic thickness is independent of the density contrast between the fluids and emerges from the requirement that the viscous flow supplied by the evolving interface must continuously match the inertial flux required to sustain front propagation. As the interface slope adjusts through viscous redistribution, a unique and stable thickness behind the front is selected, toward which the system relaxes over time. In the present configuration, this asymptotic thickness is approximately 0.2D, where D is the channel height."

Effect of channel's height

Another parameter that strongly influences the dynamics of horizontal two-dimensional lock-exchange flow is the channel height D. As introduced earlier, the equilibrium length scale given by Eq. (26) scales as $D^{\frac{5}{2}}$. While the dependence of the flow on channel height can, in principle, be derived analytically. For brevity, the trends obtained directly from the solution scheme is reported here.

The results show that when the channel height is changed from D_1 to D_2, the temporal evolution of the *normalized* front thickness collapses provided that time is rescaled according to

$$\frac{t_2}{t_1} = (\frac{D_2}{D_1})^2 \qquad (29)$$

This scaling indicates that the characteristic time governing interface evolution increases quadratically with the channel height. Here proposition 4 can be stated.

Proposition 4. Quadratic time scaling with channel height

"In horizontal two-dimensional lock-exchange flow, the temporal evolution of the normalized front thickness is governed by a viscous time scale proportional to the square of the channel height. Consequently, when the channel height changes from D_1 to D_2 identical normalized interface evolution is obtained by rescaling time as in Eq. (29)"

This scaling is independent of density contrast and indicates that channel height affects only the rate of interface evolution, not its normalized shape. Table 2 lists the time that is required after equilibrium, to reach different values of front thickness in terms of $\bar{h}$ for various channel heights. The quantities in Table. 2 only approximately demonstrate Eq. (29) because of limited precision of the algorithm used in the numerical scheme.

Table. 2. Normalized values of front thickness in $\bar{h}$ coordinates and the times required after equilibrium for different channel heights

Height (m)	$\bar{h}_f = 0.65$	$\bar{h}_f = 0.70$	$\bar{h}_f = 0.75$	$\bar{h}_f = 0.80$	$\bar{h}_f = 0.85$	$\bar{h}_f = 0.90$	$\bar{h}_f = 0.95$
0.02	0.32 s	0.69 s	1.34 s	2.55 s	5.08 s	11 s	27.3 s
0.05	2.24 s	4.66 s	8.86 s	16.6 s	32.7 s	70 s	170.5 s
0.1	8.29 s	17.87 s	34.3 s	65 s	128.2 s	277.7 s	t> 300 s
0.15	23.11 s	45.7 s	84.4 s	156.5 s	304.7 s	t>330 s	t>330 s

Conclusions

An exact analytical framework has been developed to describe horizontal lock-exchange flows by directly solving the Navier–Stokes equations under the assumption of parallel flow. The formulation provides the full temporal evolution of the interface and establishes a physically consistent coupling between the viscous flow behind the front and the inertial dynamics at the leading edge. This coupling enables prediction of the front velocity without introducing empirical closures. Several key physical propositions emerge from the analysis as follows.

First, the study demonstrates that the front thickness and the interface thickness immediately behind the front are distinct quantities governed by different mechanisms: the former is controlled by inertial momentum balance at the leading edge, whereas the latter evolves through viscous redistribution within the bulk flow. Treating these two thicknesses as identical, as is often done implicitly, obscures essential physics of lock-exchange dynamics.

Second, both the timely evolution of front thickness and the interface thickness behind the front are shown to be independent of the density contrast between the fluids in horizontal configurations. Although buoyancy determines the front velocity, it cancels identically in the coupled viscous–

inertial balance that governs thickness evolution. This result explains experimental observations in which thickness measurements collapse across a wide range of Atwood numbers.

Third, the analysis reveals that the interface thickness behind the front approaches a well-defined asymptotic fraction of the channel height. The model predicts that this thickness evolves toward a constant value, approximately 0.2D, reflecting a geometric constraint imposed by viscous redistribution rather than buoyancy effects.

Fourth, the evolution of the front thickness is shown to scale quadratically with the channel height. Specifically, identical normalized front-thickness evolution is obtained when time is scaled with D^2, demonstrating that channel geometry—rather than density contrast—sets the characteristic time scale for front development.

Comparison with controlled laboratory experiments shows good quantitative agreement in both front velocity and thickness evolution, within experimental uncertainty. Beyond providing improved predictive capability, the present framework offers a unified and physically transparent interpretation of lock-exchange flows, clarifying the respective roles of inertia, viscosity, and geometry. The methodology is readily extendable to inclined channels, non-uniform geometries, and displacement flows, providing a robust foundation for future analytical and experimental investigations.

References

[1] T. B. Benjamin, "Gravity currents and related phenomena," J. Fluid Mech. 31, 209–248 (1968).

[2] H. E. Huppert and J. E. Simpson, "The slumping of gravity currents," J. Fluid Mech. 99, 785–799 (1980).

[3] J. O. Shin, S. B. Dalziel, and P. F. Linden, "Gravity currents produced by lock exchange," J. Fluid Mech. 521, 1–34 (2004).

[4] T. Séon, J.-P. Hulin, D. Salin, B. Perrin, and E. J. Hinch, "Buoyancy-driven miscible front dynamics in tilted tubes," Phys. Fluids 17, 031702 (2005).

[5] T. Séon, J. Znaien, B. Perrin, E. J. Hinch, D. Salin, and J.-P. Hulin, “Front dynamics and macroscopic diffusion in buoyant mixing in a tilted tube,” Phys. Fluids 19, 125105 (2007).

[6] M. Ungarish, An Introduction to Gravity Currents and Intrusions (CRC Press, Boca Raton, 2009).

[7] F. Sébilleau, R. I. Issa, and S. P. Walker, “Analysis of turbulence modeling approaches to simulate single-phase buoyancy-driven counter-current flow in a tilted tube,” Flow Turbul. Combust. 96, 95–132 (2016).

[8] S. Longo, M. Ungarish, V. Di Federico, L. Chiapponi, and D. Petrolo, “Gravity currents produced by lock-release: Theory and experiments concerning the effect of a free top in non-Boussinesq systems,” Adv. Water Resour. 121, 456–471 (2018).

[9] G. Politis and J. Priede, “Lock-exchange problem for Boussinesq fluids revisited: Exact shallow-water solution,” Phys. Fluids 34, 102101 (2022).

[10] S. M. Taghavi, T. Séon, D. M. Martinez, and I. A. Frigaard, “Buoyancy-dominated displacement flows in near-horizontal channels: The viscous limit,” J. Fluid Mech. 639, 1–35 (2009).

[11] M. Yavari, M. Bazargan, N. Kazemi, E. Bagherizadeh, and J. Estevadeordal, “Front dynamics in exchange flow of two immiscible iso-viscous fluids in two-dimensional straight and curved plane channels,” Phys. Fluids 31, 092105 (2019).

[12] M. Yavari, R. Farzadi, and M. Bazargan, “Analytical solution for two-dimensional displacement flow in a curved down-sloping duct,” Phys. Fluids 32, 102110 (2020).

[13] M. Yavari, N. Kazemi, and M. Bazargan, “Comparison of exchange flow of two miscible fluids in curved and slanted straight tubes,” Eur. J. Mech. B/Fluids 101, 14–21 (2023).

[14] M. Yavari, A. Shahverdi, and M. Bazargan, “Velocity fluctuations in a lock-exchange flow at various Atwood numbers for straight and slanted channels,” ISH J. Hydraul. Eng. 30, 1–22 (2025).

[15] M. Ungarish and T. Zemach, “On the slumping of high Reynolds number gravity currents in two-dimensional and axisymmetric configurations,” Eur. J. Mech. B/Fluids 24, 71–90 (2005).

[16] M. I. Cantero, J. R. Lee, S. Balachandar, and M. H. García, “On the front velocity of gravity currents,” J. Fluid Mech. 586, 1–39 (2007).

[17] E. Meiburg and B. Kneller, “Turbidity currents and their deposits,” Annu. Rev. Fluid Mech. 42, 135–156 (2010).

[18] M. van Reeuwijk, M. Holzner, and C. P. Caulfield, “Mixing and entrainment are suppressed in inclined gravity currents,” J. Fluid Mech. 873, 786–815 (2019).

[19] P. A. Allen, R. M. Dorrell, O. G. Harlen, R. E. Thomas, and W. D. McCaffrey, “Mixing in density- and viscosity-stratified flows,” Phys. Fluids 34, 056602 (2022).

[20] S. M. Taghavi, T. Séon, K. Wielage-Burchard, D. M. Martinez, and I. A. Frigaard, “Stationary residual layers in buoyant Newtonian displacement flows,” Phys. Fluids 23, 044105 (2011).

[21] T. von Kármán, “The engineer grapples with nonlinear problems,” Bull. Am. Math. Soc. 46, 615–683 (1940).

[22] V. K. Birman, B. A. Battandier, E. Meiburg, and P. F. Linden, “Lock-exchange flows in sloping channels,” J. Fluid Mech. 577, 53–77 (2007).

[23] K. Alba, S. M. Taghavi, and I. A. Frigaard, “Miscible density-unstable displacement flows in inclined tubes,” Phys. Fluids 25, 067101 (2013).

[24] A. Dai and Y.-L. Huang, “The flow within the head of a gravity current,” J. Fluid Mech. 997, A42 (2024).

[25] M. Yavari, R. Ehteshami, N. Kazemi, and M. Bazargan, “An experimental study of transient front velocity for miscible exchange flow in a rectangular channel,” ISH J. Hydraul. Eng. 30, 679–695 (2024).